Utilizing *in situ* Electrochemical SHINERS for Oxygen Reduction Reaction Studies in Aprotic Electrolytes

Thomas A. Galloway and Laurence J. Hardwick*

Stephenson Institute for Renewable Energy, Department of Chemistry, University of Liverpool, Liverpool, L69 7ZD

AUTHOR INFORMATION

Corresponding Author

* E-mail: hardwick@liverpool.ac.uk

ABSTRACT

Spectroscopic detection of reaction intermediates upon a variety of electrode surfaces is of major interest within physical chemistry. A notable technique in the study of the electrochemical interface has been surface enhanced Raman spectroscopy (SERS). The drawback of SERS is that it is limited to roughened gold and silver substrates. Herein we report that shell-isolated nanoparticles for enhanced Raman spectroscopy (SHINERS) can overcome the limitations of SERS and has followed the oxygen reduction reaction (ORR), within a non-aqueous electrolyte, on glassy carbon, gold, palladium and platinum disk electrodes. The work presented demonstrates SHINERS for spectro-electrochemical studies for applied and fundamental electrochemistry in aprotic electrolytes, especially for the understanding and development of future metal-oxygen battery applications. In particular we highlight that with the addition of Li^+, both the electrode surface and solvent influences the ORR mechanism, which opens up the possibility of tailoring surfaces to produced desired reaction pathways.

TOC GRAPHICS

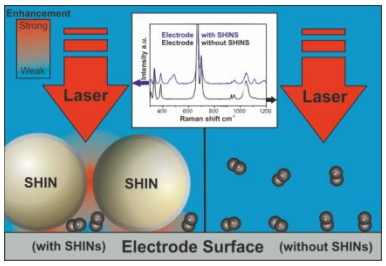

Understanding the electrochemistry of oxygen in non-aqueous electrolyte media is of great interest in particular for the development of metal-air batteries[1,2], where the formulation of a stable electrolyte is a major challenge and so far inhibiting its development.[3-5]. The oxygen reduction and oxidation reaction mechanisms can be complex, involving multiple intermediates and are highly dependent upon the solvent used.[5,6] There have been a number of recent studies on the development of the electrolyte media[8,9], using a variety of analytical and spectroscopic techniques.[9-12] In particular, surface enhanced Raman spectroscopy (SERS)[13] has been shown to be a valuable technique, however it is limited by the surfaces that it can be used to analyze, essentially gold and silver.[14,15]

The Raman effect is very weak (1 photon in ca. 10 million is inelastically scattered)[16]. The signal can be enhanced up to ca. 10^{11} by roughening the electrode surface, using an electrochemical oxidation/reduction cycle (ORC).[17] SERS is a non-destructive and non-invasive technique; it can be used to investigate the chemical bonding of surface species, making it a valuable technique to study *in situ* the oxygen reduction and evolution reactions (ORR and OER) taking place at the electrode interface.[18] SERS has been used to study the ORR and OER reaction on Au in metal-oxygen batteries[19] and has shown the effect of varying the alkyl chain length in the supporting salt.[20] SERS studies with respect to ORR have so far been limited in the main to Au surfaces, but there is significant interest to study these reactions on non-SERS surfaces, such as carbon, a prominent option as a future cathode material.[21] Unlike SERS the use of SHINERs (shell isolated nanoparticles for enhanced Raman spectroscopy) is not restricted to precious metal surfaces. Adding a near-monolayer of SHINs can enhance the Raman signal by ca. 10^8.[22] SHIN's consist of a gold core, surrounded by a very thin (2-3 nm) uniform SiO_2 shell (**Figure 1**). The shell thickness is very important; a shell greater than 4 nm will drastically reduce the

enhancement from the Au core (**Figure S1.1**). The gold nanoparticle has a strong electromagnetic field that enhances the Raman signal, whilst the SiO_2 shell inhibits any catalytic effect from the gold core[23]. The greatest enhancement from nanoparticles occurs between two SHINERS particles where the electromagnetic field from both cores can enhance the nearby molecules, as indicated by the red areas on the scheme (**Figure 1a**). SHINERs can therefore enhance the Raman signal upon a variety of surfaces,[24,25] such as carbon that has previously been very challenging to analyze. Validation of uniform silica coating and application of SHINERS are discussed in **Figures S1.1-S1.5** and **Table S1**.

Studying the ORR using 0.1 M $TBAClO_4$ in dimethyl sulfoxide (DMSO) on a smooth polycrystalline gold electrode demonstrated that Raman spectroscopy on a surface without any enhancement is inherently weak (**Figure 2a**). The spectrum at open circuit voltage (OCV) displays DMSO solvent peaks. No spectral bands were observed for the supporting salt. The lack of peaks is likely a result of no surface plasmons to enhance the inelastically scattered photons of surface adsorbed tetrabutylammonium (TBA). Raman scans were taken at decreasing potentials down to 1.84 V. There was no change observed in peak position or intensity from the OCV spectrum at any potential.

The Au surface can be electrochemically roughened prior to experiments using an oxidation-reduction cycle; this created a nanostructured surface, which leads to a distribution of charge when excited by photons[26], enhancing the local electric field. The chemically adsorbed molecules can also undergo charge transfer with the surface that can in turn increase the polarizability[27]. Roughening the surface displays a notable enhancement (**Figure 2b**). The same electrochemical system as **Figure 2a** was used with a roughened gold electrode. At open circuit voltage (OCV) only peaks related to DMSO were visible. The growth of two bands at 1110 cm^{-1}

(υ_{O-O}) and 490 cm^{-1} (υ_{Au-O}) were observed when the potential was decreased and can be assigned to the formation of adsorbed superoxide (O_2^-). The position of these peaks agrees well with literature.[19,28] To confirm the origin of the observed peaks, the experiment was run without the presence of oxygen, under argon. (**Figure S2**) and no peaks are seen to grow in either the O_2^- or Au-O spectral region, within similar potential cycling limits.

SHINs are an alternative method of enhancing the Raman signal of substrate molecules on the electrode surface. In the same 0.1 M $TBAClO_4$/DMSO electrolyte media the *in situ* reaction on a smooth polycrystalline gold electrode was studied with 2 μl of SHINs drop cast onto the surface (**Figure S3**). The OCV Raman spectrum only showed DMSO solvent peaks in agreement with the polycrystalline surface with and without surface enhancement. The *in situ* Raman spectra **(Figure 2c**) between 2.84 V and 1.84 V observed the growth of two peaks at 1110 cm^{-1} and 490 cm^{-1} for the free O_2^- and gold oxide peaks.[20] A comparison of the two sets of spectra for SERS and SHINERS demonstrated that SHINERS is a useful technique to monitor the ORR in a non-aqueous electrolyte media, without loss of signal intensity from the different method of phonon enhancement and has been shown to provide similar data in different anion salt electrolytes, such as in tetrabutylammonium triflate (**Figure S4**). Furthermore **Figure S5** shows that SHINs have no effect on the electrochemistry as the electrochemical response with and without SHINS is identical.

The electrochemistry of 0.1 M $TBAClO_4$ in DMSO saturated with oxygen varies between different electrode surfaces (**Figure 3**). The reversibility of the O_2^- couple is affected when the electrode surface is changed. Glassy carbon (GC) is the most reversible (ΔE = 90 mV), whereas platinum is the least reversible (ΔE = 350 mV). The change in reversibility is accounted for by the interactions of O_2^- with the surface, whereby Pt has the slowest reaction kinetics of the three

surfaces (Pt < Pd < Au), with O_2^- being the most strongly chemisorbed, which is in agreement with density function theory calculations, where O_2^- is energetically favorable to chemisorb to the Pt surface.[29] There is little interaction with the surface on the GC electrode, unlike Au, Pd and Pt, where dioxygen can chemisorb.[29] Pt has the strongest interaction with O_2^- due to the bonding of the $5d_{xx}$ and O_2^- $2\pi^*$ orbitals in Pt, giving a higher adsorption energy and shorter metal-oxygen bond length than with Au. Au has a filled d orbital so O_2^- is not chemisorbed like Pt; a weaker interaction still occurs due to a distortion of charge density creating an overlap of bonding orbitals.[29] The same principle is applied for Pd (bonding of the $4d_{xx}$ and O_2^- $2\pi^*$ orbitals), however Pd has a lower oxygen binding energy than Pt.[30] Previous studies have shown similar behavior on GC electrodes with different solvent electrolytes such as dimethyl ether where a change in reversibility is observed due to the different solubility and kinetics, but a $1e^-$ reduction mechanism is still observed.[31]

The Pd surface exhibits similar behavior to the Au surface for the ORR (**Figure 4a**). A peak at 1108 cm^{-1} for O_2^- is observed from 2.74 V and grows in intensity with negative potential, correlating with cyclic voltammetry data in **Figure 3**. A corresponding peak at 486 cm^{-1} for (υ_{Pd-O}) grows proportionally to the O_2^- peak. The *in situ* Raman spectra on Pt (**Figure 4b**) showed a variance in the spectral response in comparison to Au and Pd. At 1108 cm^{-1} a peak assigned to υ_{O-O} of O_2^- grew in intensity with increasing reduction potential, similar to that observed on Au and Pd. However, on Pt unlike Au and Pd the interaction with the Pt surface was different. Initially on the Pt surface a peak was observed at the lower wavenumber of 456 cm^{-1} and initially grew in intensity with decreasing potential. A second peak at 484 cm^{-1} grew at more negative potentials at the expense of the 456 cm^{-1} peak which then decreased in intensity. In both **Figures**

2c and 4b, a small band at 1179 cm^{-1} is observed to appear (and diminish in the case of Pt); its assignment will be discussed later within this paper.

The SHINERS data demonstrates variation of O_2^- interaction between Pt and the other two metal surfaces (**Figure S6 and Table S2**). All three surfaces exhibit a shoulder at 456 cm^{-1}, for Au and Pd this remains a shoulder on the peak around 490 cm^{-1}. Pt favors the peak at 456 cm^{-1} at lower reduction potentials, as the potential decreases the peak at 490 cm^{-1} becomes dominant. It is likely the two peaks originate from different vibrational stretching modes of O_2^- adsorbed on the metal surface[32]. At lower potentials, there is a lower surface coverage of O_2^- on the Pt allowing the O_2^- to have a flat orientation; with increasing negative reduction potentials, an end on orientation is favored. This could account for the flat conformation rather than the end on conformation on Pt, unlike Au and Pd, which favor the end on conformation due to a weaker interaction with the surface of the electrode[29]. Furthermore the interaction of the solvent with the electrode surface also needs to be taken into account; at less negative potentials DMSO may passivate the surface, preventing the onset of dioxygen adsorption. Future studies using single crystal electrodes with SHINERS would be required to clarify the exact mechanism taking place at the platinum surface, in combination with appropriate level theory calculations.

The GC surface exhibits different behavior to the metal surfaces analyzed previously (**Figure 5**). There was no Raman peak observed between 400 and 550 cm^{-1} at any potential on the GC electrode surface. Thereby there is an absence of a metal-O_2^- interaction (area indicated via a #) and this indicates that the SHINERS particles are pinhole free (**Figure S1.1-S1.4**). This provides strong verification that the O_2^- peak ($\upsilon_{O\text{-}O}$) at ∽1110 cm^{-1} originates solely from its interaction at the GC surface, not with the gold core of the SHIN, with it being detected solely due to the Raman enhancement from the SHIN particles. The formation of O_2^- on the GC surface occurred

below 2.84 V in the reduction sweep at 1107 cm^{-1}, the band shifts positively to 1123 cm^{-1} with decreasing potential.[33] At lower potential, O_2^- is bound at more favorable sites on the surface, with increasing concentration O_2^- is forced into less favorable sites, reducing the interaction with the surface causing a positive shift in the Raman band, this coincides with a peak at 1520 cm^{-1} that could be a result of the interaction of O_2^- with the graphitic rings in the carbon.[34] The interaction of the O_2^- with the graphitic ring could increase with decreasing potential, creating greater distortion with the ring and accounting for the wavenumber shift of the O_2^- peak. **Figure S7** confirms that the 1520 cm^{-1} band is unique to carbon substrate as it is not observed on Au within an extended wavenumber range.

SHINERS on GC also displayed bands at 1179, (as seen in **Figures 2c** and **4b**) 1230 and 1450 cm^{-1} that coincide with ORR (**Figure 5**). No potential dependent electrolyte bands could be assigned to these peaks, nor known reduced oxygen salts (**Figures S8 and S9**).[20] We speculate that 1179 cm^{-1} could be assigned to HO_2, as its position is close the band at 1165 cm^{-1} identified by the group of Gewirth of HO_2 adsorbed onto Au in perchloric acid ($HClO_4$) solution.[35] Concurrently the band at 1450 cm^{-1} can be then tentatively assigned as νHO_2-C, with the band at 1230 cm^{-1} remaining as yet unassigned. Strict drying protocol ensured that all measurements took place in H_2O content below 20 ppm, as determined by Karl Fisher titration. Thereby we believe the nature of the measurements is sensitive to trace water contamination. Certainly further investigations using SHINERS to understand the effect of water concentration on these bands, with the use of isotopic labelling to strengthen band assignments is warranted.

SHINERS was then employed to investigate ORR in the presence of Li^+ in low (acetonitrile – MeCN) and high (DMSO) donor number solvents, with corresponding electrochemistry in **Figure S10**. In 0.5 M $LiClO_4$, MeCN (**Figure 6a**), SHINERS detected the growth of LiO_2 at

1125 cm^{-1} on GC below 2.84 V, with Li_2O_2 not detected, due to the absence of the main peroxide band at 790 cm^{-1}. In addition, a peak at 1500 cm^{-1} was observed in the MeCN Raman spectra at lower reduction potentials. This peak is likely the result of LiO_2 interacting with a vibrational mode of the graphitic ring[34] (**Table S3**). SHINERS on GC in 0.5 M $LiClO_4$, DMSO (**Figure 6b**) showed the appearance of Li_2O_2 at 790 cm^{-1} at 2.74 V, which remained as the potential decreased further to 1.74 V. At 2.74 V bands pertaining to LiO_2 at 1128 cm^{-1} and LiO_2-C at 1500 cm^{-1} were also detected on the GC electrode. The appearance of LiO_2 is indicative of a mechanism where both Li_2O_2 and LiO_2 are formed as stable products on the GC surface. The proposed decomposition reaction of DMSO to dimethyl sulfone ($DMSO_2$) was unable to be established in our measurements, due to the absence of a peak around 1142 cm^{-1}.[36]

The data reported herein on GC is suggestive of a reaction mechanism that is both surface and solvent dependent. The solvation of the Li^+ cation in MeCN is lower due to a positive Gibbs free energy, therefore ORR occurs on the surface and LiO_2 will be observed on the electrode[19] (equations 1 and 2). The interaction of LiO_2 with the carbon surface appears to stabilize the adsorbed LiO_2 species and within the experiment, no Li_2O_2 formation is observed to occur from a second electron transfer or via disproportionation. This observation agrees with work of Lu et al.[37] that shows the stabile cycling of LiO_2. In DMSO (equations 1, 3 and 4), a partial surface/solution mechanism occurs, whereby both Li_2O_2 and LiO_2 are formed as the major reduction products, which is contrary to what has been reported on Au electrode subtrates[19]. LiO_2 is also bound to the carbon surface in DMSO (1500 cm^{-1}). LiO_2 can then desorb and diffuse into the bulk electrolyte, where it can disproportionate to give Li_2O_2 in agreement with data published by Ye et al.[38] Li_2CO_3 was not detected during ORR on GC, implying the decomposition of the carbon electrode was negligible during the time frame of the measurement (**Figure S9**).

$$O_2 + e^- \rightarrow O_2^-{}_{(ads)} \quad (1)$$

$$Li^+ + O_2^-{}_{(ads)} \rightarrow LiO_{2(ads)} \quad (2)$$

$$Li^+ + O_2^- \rightarrow LiO_{2(ads)} \leftrightarrows [Li^+\text{--}O_2^-]_{(sol)} \quad (3)$$

$$[Li^+\text{--}O_2^-]_{(sol)} + [Li^+\text{--}O_2^-]_{(sol)} \rightarrow Li_2O_{2\,(s)} + O_2 \quad (4)$$

SHINERS has been demonstrated as an effective method of detecting intermediate species and ORR products on an array of electrode substrates, such as Pt, Pd and GC, which previously SERS has been unable to access. The consistency of SHINERS has been validated by its ability to reproduce data gathered using SERS in the same electrolyte media on Au electrode surfaces. Notably the metal-superoxide band shape varies between the noble metals depending on superoxide interaction at the surface. The use of SHINERS in the presence of Li^+ has shown that both surface and solvent can be harnessed to influence ORR pathways, which may be critical in designing electrode/electrolyte interfaces that can minimize side reactions within Li-O_2 cells. This work provides a strong platform to study more complex electrolyte and electrode systems with SHINERS particles.

ASSOCIATED CONTENT

The following files are available free of charge

Methods section, SHIN preparation, synthesis and validation, transfer onto electrode surfaces and enhancement factor of SHIN particles. Supporting electrochemical data, Raman spectra of materials used, and Raman peak analysis comparison of superoxide on metal surfaces. SERS and SHINERS experiments under argon deoxygenated electrolytes.

AUTHOR INFORMATION

Notes

The authors declare no competing financial interests.

ACKNOWLEDGMENT

Professor Jian-Feng Li and Jin Chao Dong (Xiamen University) are acknowledged for their knowledge and assistance and access to their facilites in learning the synthesis and procedure for SHINERS. Professor Richard Nichols and the Electronanomat Exchange Program are acknowledged. Dr Sarah Ball, Dr Mark Copley, Johnson Matthey and the Engineering and Physical Sciences Research Council (EPSRC) CASE award are acknowledged. Dr Tobias Heil and the Nanoinvestigation Centre at Liverpool (NiCaL) are acknowledged for access to their TEM. Support from the EPSRC grant EP/J020265/1 is also gratefully acknowledged.

REFERENCES

(1) Cheng, F.; Chen, J. Metal-Air Batteries: From Oxygen Reduction Electrochemistry to Cathode Catalysts. *Chem. Soc. Rev.* **2012**, *41*, 2172-2192.

(2) Rahman, M. A.; Wang, X.; Wen, C. High Energy Density Metal-Air Batteries: A Review. *J. Electrochem. Soc*. **2013**, *160*, A1759-A1771.

(3) Bruce, P.G.; Freunberger, S.A.; Hardwick, L. J.; Tarascon, J. M. Li-O_2 and Li-S Batteries with High Energy Storage. *Nat. Mater*. **2012**, *11*, 19-29.

(4) Tarascon, J. M. Key Challenges in Future Li-Battery Research. *Philos. Trans. R. Soc., A.* **2010**, *368*, 3227-3241.

(5) Girishkumar, G.; McCloskey, B.; Luntz, A. C.; Swanson, S.; Wilcke, W. Lithium-Air Battery: Promise and Challenges. *J. Phys. Chem. Lett.* **2010**, *1*, 2193-2203.

(6) *Zhang, J.; PEM Fuel Cell Electrocatalysts and Catalyst Layers: Fundamentals and Applications.* Springer London; 2008.

(7) Sawyer, D. *Oxygen Chemistry*. Oxford University Press*, USA*; 1991.

(8) Lodge, A. W.; Lacey, M. J.; Fitt, M.; Garcia-Araez, N.; Owen, J. R. Critical Appraisal on the Role of Catalysts for the Oxygen Reduction Reaction in Lithium-Oxygen Batteries. *Electrochim. Acta.* **2014**, *140*, 168-173.

(9) Padmanabhan, V. J.; Berry, N. G.; Papageorgiou, G.; Nichols, R. J.; Hardwick, L. J. Mechanistic Insight into the Superoxide Induced Ring Opening in Propylene Carbonate Based Electrolytes using in situ Surface-Enhanced Infrared Spectroscopy. *J. Am. Chem. Soc.* **2016**, *138*, 3745-3751.

(10) Peng, Z. Q.; Freunberger, S. A.; Hardwick, L. J.; Chen, Y. H.; Giordani, V.; Barde, F.; Novak, P.; Graham, D.; Tarascon, J. M.; Bruce, P. G. Oxygen Reactions in a Non-Aqueous Li^+ Electrolyte. *Angew. Chem. Int. Ed.* **2011**, *50*, 6351-6355.

(11) Sharon, D.; Etacheri, V.; Garsuch, A.; Afri, M.; Frimer, A. A.; Aurbach, D. On the Challenge of Electrolyte Solutions for Li-Air Batteries: Monitoring Oxygen Reduction and Related Reactions in Polyether Solutions by Spectroscopy and EQCM. *J. Phys. Chem. C.* **2013**, *4*, 127-131.

(12) Trahan, M. J.; Mukerjee, S.; Plichta, E. J.; Hendrickson, M. A.; Abraham, K. M. Studies of Li-Air Cells Utilizing Dimethyl Sulfoxide-Based Electrolyte. *J. Electrochem. Soc.* **2013**, *160*, A259-A267.

(13) Mozhzhukhina, N.; Méndez De Leo, L. P.; Calvo, E. J. Infrared Spectroscopy Studies on Stability of Dimethyl Sulfoxide for Application in a Li–Air Battery. *J. Phys. Chem. C.* **2013**, *117*, 18375-18380.

(14) Tian, Z. Q. Surface-enhanced Raman spectroscopy: advancements and applications. *J. Raman. Spectrosc.* **2005**, *36*, 466-470.

(15) Gittleson, F. S.; Yao, K. P. C.; Kwabi, D. G.; Sayed, S. Y.; Ryu, W. H.; Shao-Horn, Y.; Taylor, A. D. Raman Spectroscopy in Lithium–Oxygen Battery Systems. *J. Am. Chem. Soc*. **2015**, *2*, 1446-1457.

(16) Otto, A.; Mrozek, I.; Grabhorn, H.; Akemann, W. Surface Enhanced Raman Scattering. *J. Phys.: Cond. Matter.* **1992**, *4*, 1143-1212.

(17) Wu, D.-Y.; Li, J.-F.; Ren, B.; Tian, Z. Q. Electrochemical Surface-Enhanced Raman Spectroscopy of Nanostructures. *Chem. Soc. Rev.* **2008**, *37*, 1025-1041.

(18) Laoire, C. O.; Mukerjee, S.; Abraham, K. M.; Plichta, E. J.; Hendrickson, M. A. Elucidating the Mechanism of Oxygen Reduction for Lithium-Air Battery Applications. *J. Phys. Chem. C.* **2009**, *113*, 20127-20134.

(19) Johnson, L.; Li, C. M.; Liu, Z.; Chen, Y. H.; Freunberger, S. A.; Ashok, P. C.; Praveen, B. B.; Dholakia, K.; Tarascon, J. M.; Bruce, P. G. The role of LiO_2 Solubility in O_2 Reduction in Aprotic Solvents and its Consequences for LiO_2 Batteries. *Nat. Chem.* **2014**, *6*, 1.

(20) Aldous, I. M.; Hardwick, L. J. Influence of Tetraalkylammonium Cation Chain Length on Gold and Glassy Carbon Electrode Interfaces for Alkali Metal-Oxygen Batteries. *J. Phys. Chem. Lett.* **2014**, *5*, 3924-3930.

(21) Hardwick, L. J.; Bruce, P. G. The Pursuit of Rechargeable Non-Aqueous Lithium-Oxygen Battery Cathodes. *Current Opinion in Solid State & Materials Science.* **2012**, *16*, 178-185.

(22) Li, J. F.; Huang, Y. F.; Ding, Y.; Yang, Z. L.; Li, S. B.; Zhou, X. S.; Fan, F. R.; Zhang, W.; Zhou, Z. Y.; Wu, D. Y.; Ren, B.; Wang, Z. L.; Tian, Z. Q. Shell-Isolated Nanoparticle-Enhanced Raman Spectroscopy. *Nature.* **2010**, *464*, 392-395.

(23) Li, J. F.; Tian, X. D.; Li, S. B.; Anema, J. R.; Yang, Z. L.; Ding, Y.; Wu, Y. F.; Zeng, Y. M.; Chen, Q. Z.; Ren, B.; Wang, Z. L.; Tian, Z. Q. Surface Analysis using Shell-Isolated Nanoparticle-Enhanced Raman Spectroscopy. *Nat. Protoc*. **2013**, *8*, 52-65.

(24) Huang, Y.-F.; Li, C.-Y.; Broadwell, I.; Li, J. F.; Wu, D. Y.; Ren, B.; Tian, Z. Q. Shell-Isolated Nanoparticle-Enhanced Raman Spectroscopy of Pyridine on Smooth Silver Electrodes. *Electrochimica. Acta.* **2011**, *56*, 10652-10657.

(25) Li, J. F.; Ding, S. Y.; Yang, Z. L.; Bai, M. L.; Anema, J. R.; Wang, X.; Wang, A.; Wu, D. Y.; Ren, B.; Hou, S. M.; Wandlowski, T.; Tian, Z. Q. Extraordinary Enhancement of Raman Scattering from Pyridine on Single Crystal Au and Pt Electrodes by Shell-Isolated Au Nanoparticles. *J. Am. Chem. Soc.* **2011**, *133*, 15922-15925.

(26) Kneipp, K.; Moskovits, M.; Kneipp, H. *Surface-Enhanced Raman Scattering: Physics and Applications.* Physica-Verlag; 2006.

(27) Aroca, R. *Surface-Enhanced Vibrational Spectroscopy*. Wiley; 2006.

(28) Socrates, G. *Infrared and Raman Characteristic Group Frequencies: Tables and Charts. Wiley;* 2001.

(29) Zhuang, G. V.; Markovic, N. M.; Ross P.N., Meeting, E. S. Power Source Modeling: Proceedings of the International Symposium. Proc. - Electrochem. Society. 2002, 30, 63-73.

(30) Norskov, J .K.; Rossmeisl, J.; Logadottir, A.; Lindqvist, L.; Kitchin, J. R.; Bligaard, T.; Jonsson, H. Origin of the Overpotential for the Oxygen Reduction at a Fuel-Cell Cathode. *J. Phys. Chem. B*. **2004**, *108*, 17886-17892.

(31) Laoire, C. O.; Mukerjee, S.; Abraham, K. M. Influence of Non-Aqueous Solvents on the Electrochemistry of Oxygen in the Rechargeable Lithium-Air Battery. *J. Phys. Chem. C.* **2010**, *114*, 9178-9186.

(32) McBride, J. R.; Graham, G. W.; Peters, C. R.; Weber, W. H. Growth and Characterization of Reactively Sputtered Thin-Film Platinum Oxides. *J. Appl. Phys.* **1991**, *69*, 1596-1604.

(33) Yang, H. H.; McCreery, R. L. Elucidation of the Mechanism of Dioxygen Reduction on Metal-Free Carbon Electrodes. *J. Electrochem. Soc.* **2000**, *147*, 3420-3428.

(34) Zhai, D.; Wang, H. H.; Lau, K. C.; Gao, J.; Redfern, P. C.; Kang, F.; Li, B.; Indacochea, E.; Das, U.; Sun, H.; Sun, H. H.; Amine, K.; Curtiss, L. A. Raman Evidence for Late Stage Disproportionation in a Li-O_2 Battery. *J. Phys. Chem. C.* **2014**, *5*, 2705-2710.

(35) Li, X.; Gewirth, A. Oxygen Electroreduction through a Superoxide Intermediate on Bi-Modified Au Surfaces. *J. Am. Chem. Soc.* **2005**, *127*, 5252-5260.

(36) Schroeder, M. A.; Kumar, N.; Pearse, A. J.; Liu, C.; Lee, S. B.; Rubloff, G. W.; Leung, K.; Noked, M. DMSO-Li_2O_2 Interface in the Rechargeable Li-O_2 Battery Cathode: Theoretical and Experimental Perspectives on Stability. *ACS Appl. Mater. Interfaces*. **2015**, *5*, 11402-11411.

(37) Lu, J.; Lee, Y. J.; Luo, X.; Lau K. C.; Asadi, M.; Wang, H. H.; Brombosz, S.; Wen, J.; Zhai, D.; Chen, Z.; et al. A Lithium-Oxygen Battery based on Lithium Superoxide. *Nature*. **2016**, *529*, 377-382.

(38) Qiao, Y.; Ye, S. Spectroscopic Investigation for Oxygen Reduction and Evolution Reactions on Carbon Electrodes in Li-O_2 Battery. *J. Phys. Chem. C.* **2016,** *120*, 8033-8047.

Figure Captions

Figure 1 (a) Schematic diagram of SHINs on a substrate showing the electromagnetic field distribution between SHINs (see the graduated color key where red=strong and green = weak enhancement). TEM images (b), (c) of SHINs at different resolutions with a 2 nm shell and (d) example of a 3.5 nm shell particle.

Figure 2 *In situ* Raman spectra of the ORR in 0.1 M $TBAClO_4$/DMSO electrolyte on (a) smooth (b) roughened (c) SHIN's drop cast on the surface of a polycrystalline gold electrode. All potentials vs Li/Li^+ (SHINERS particles and adsorbed dioxygen are not drawn to scale).

Figure 3 Cyclic voltammograms of 0.1 M $TBAClO_4$ in DMSO at 50 m V/s on various electrode surfaces.

Figure 4 *In situ* Raman spectra of 0.1 M $TBAClO_4$ in DMSO saturated with O_2 on (a) Pd and (b) Pt with SHINs drop cast onto the surface. All potentials vs Li/Li^+.

Figure 5 *In situ* Raman spectra of 0.1 M $TBAClO_4$ / DMSO with O_2 on a GC electrode with SHINS drop cast onto the electrode surface. Potentials vs. Li/Li^+.

Figure 6 *In situ* Raman spectra on a GC electrode with SHIN's in 0.5 M $LiClO_4$ in (a) MeCN (b) DMSO. All potentials vs. Li/Li^+.

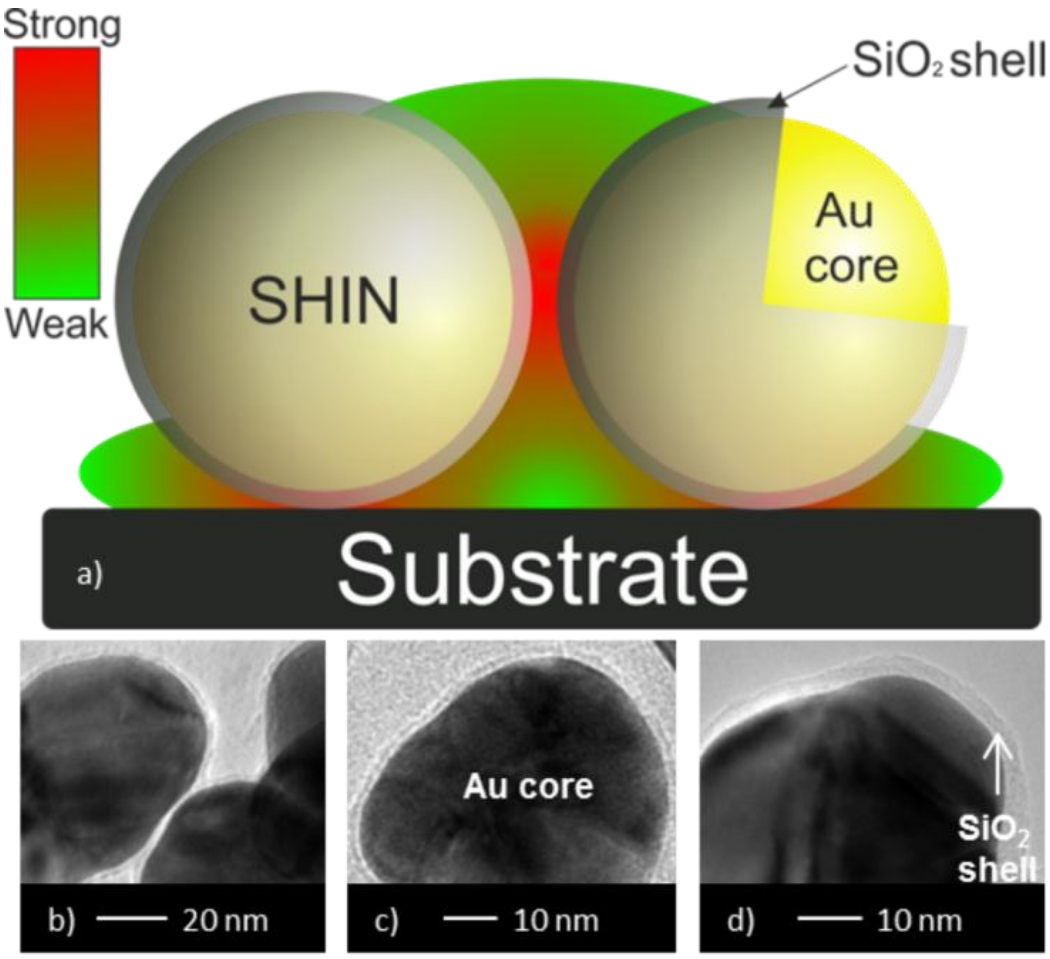
Strong
Weak
SiO₂ shell
SHIN
Au
core
a)
Substrate
Au core
SiO₂
shell
b) 20 nm
c) 10 nm
d) 10 nm

Figure 1

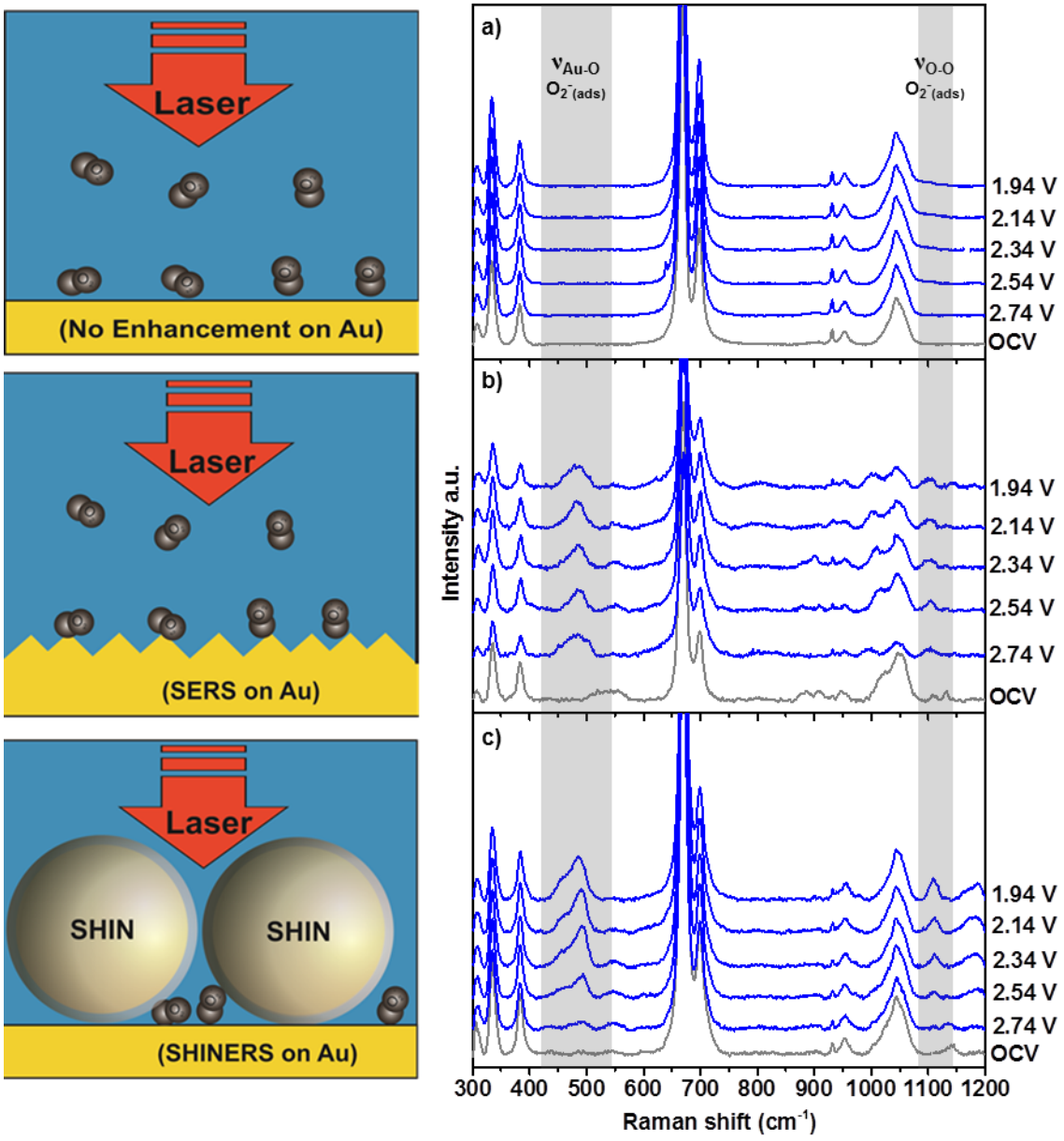
Laser
(No Enhancement on Au)
Laser
(SERS on Au)
Laser
SHIN
SHIN
(SHINERS on Au)
a)
b)
c)
ν_{Au-O} O_2^-(ads)
ν_{O-O} O_2^-(ads)
1.94 V
2.14 V
2.34 V
2.54 V
2.74 V
OCV
Intensity a.u.
300 400 500 600 700 800 900 1000 1100 1200
Raman shift (cm^{-1})

Figure 2

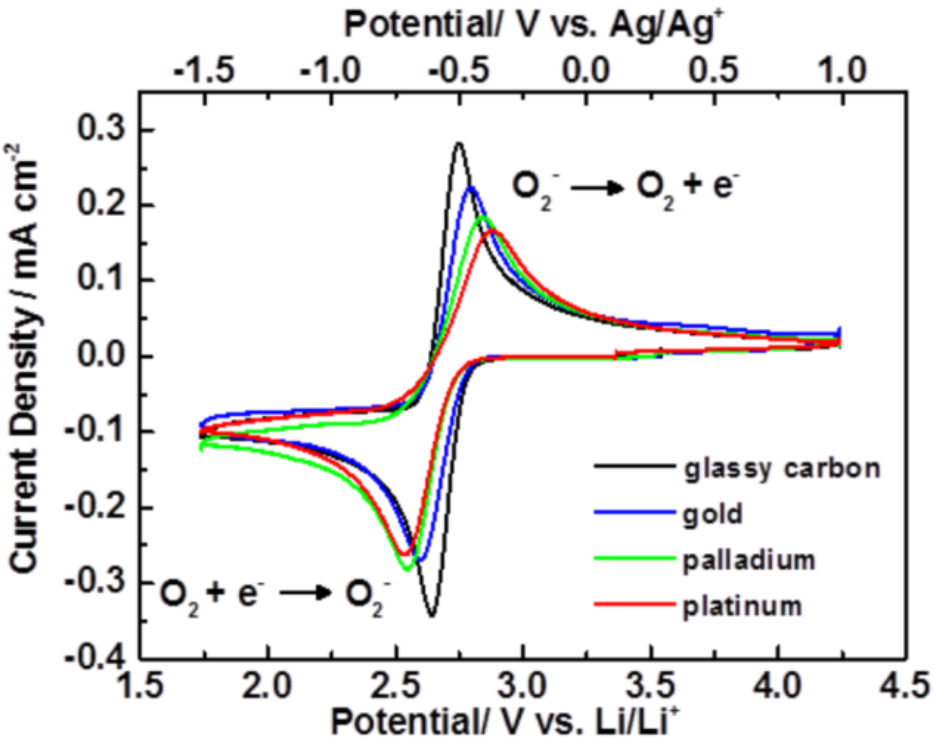
Potential/ V vs. Ag/Ag+
-1.5
-1.0
-0.5
0.0
0.5
1.0
Current Density / mA cm-2
0.3
0.2
0.1
0.0
-0.1
-0.2
-0.3
-0.4
O2- → O2 + e-
O2 + e- → O2-
glassy carbon
gold
palladium
platinum
1.5
2.0
2.5
3.0
3.5
4.0
4.5
Potential/ V vs. Li/Li+

Figure 3

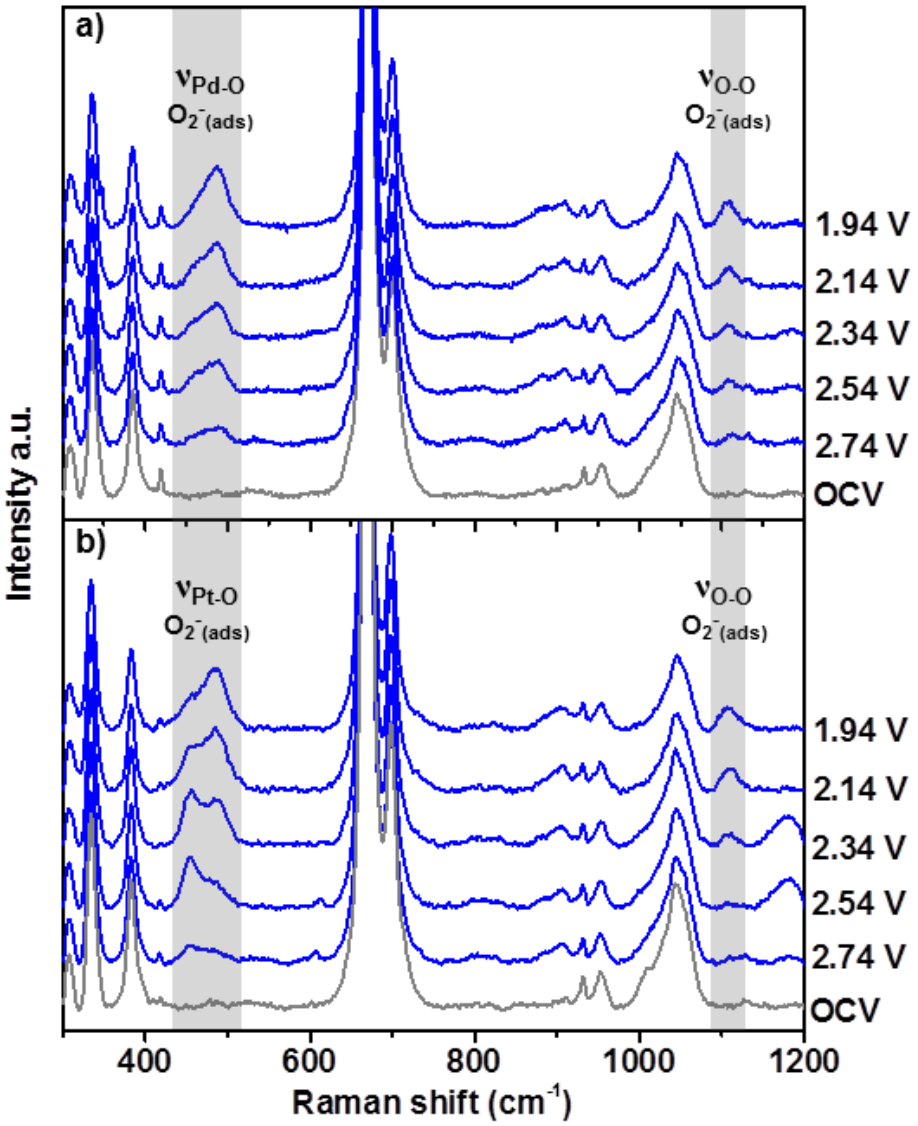
a)
ν_{Pd-O}
O_2^-(ads)
ν_{O-O}
O_2^-(ads)
1.94 V
2.14 V
2.34 V
2.54 V
2.74 V
OCV
b)
ν_{Pt-O}
O_2^-(ads)
ν_{O-O}
O_2^-(ads)
1.94 V
2.14 V
2.34 V
2.54 V
2.74 V
OCV
Intensity a.u.
400
600
800
1000
1200
Raman shift (cm^{-1})

Figure 4

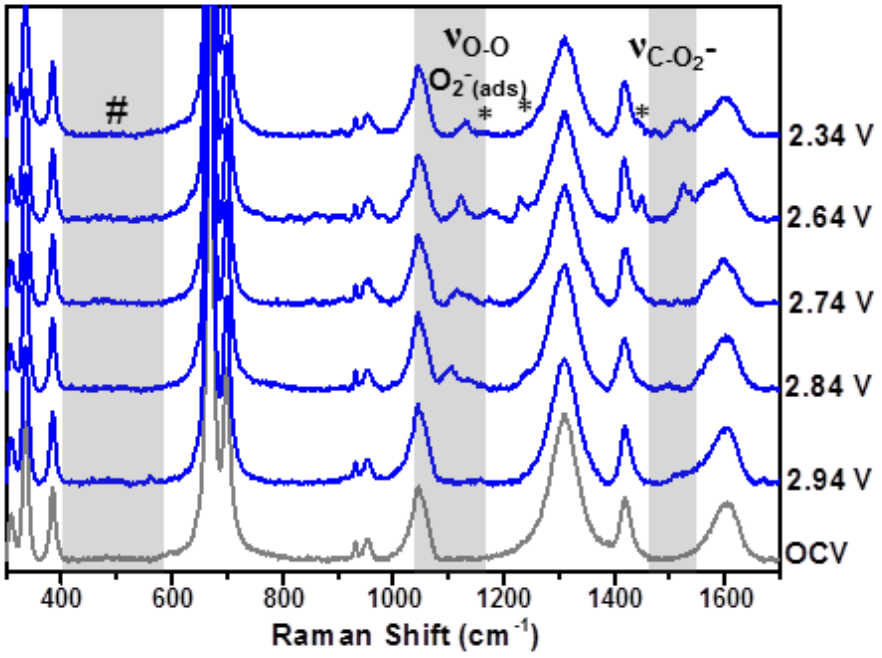
#
ν_{O-O}
O_2^- (ads)
ν_{C-O_2}-
*
*
*
2.34 V
2.64 V
2.74 V
2.84 V
2.94 V
OCV
400
600
800
1000
1200
1400
1600
Raman Shift (cm^{-1})

Figure 5

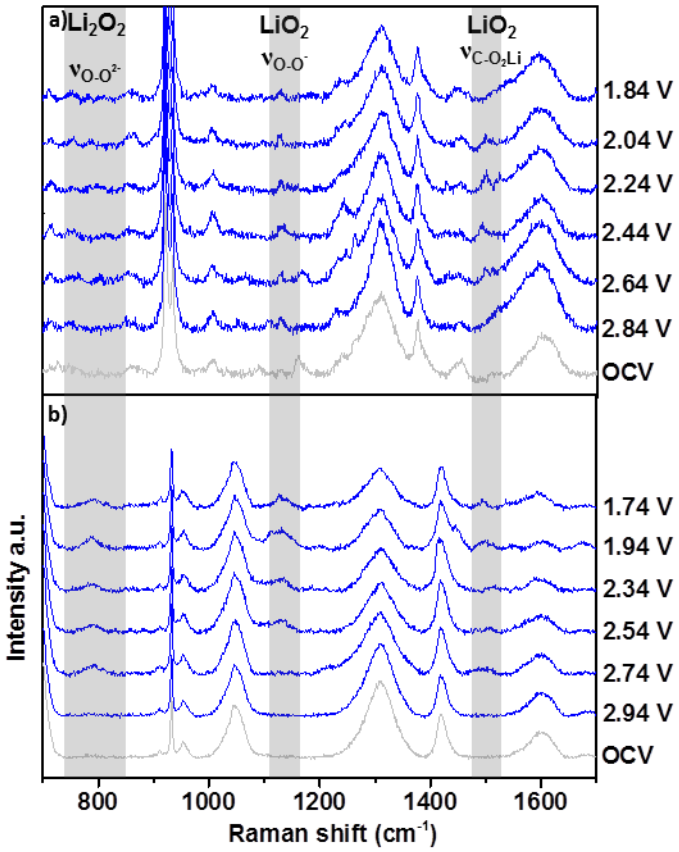
a)Li2O2
νO-O2-
LiO2
νO-O-
LiO2
νC-O2Li
1.84 V
2.04 V
2.24 V
2.44 V
2.64 V
2.84 V
OCV
b)
1.74 V
1.94 V
2.34 V
2.54 V
2.74 V
2.94 V
OCV
Intensity a.u.
800
1000
1200
1400
1600
Raman shift (cm-1)

Figure 6